Original Research

Effects of Dopant Concentration and Temperature on Upconversion Photoluminescence of Textured $CaBi_4Ti_4O_{15}$: Yb^{3+}, Ho^{3+} Ceramics

Zhen Liu [1], Kai Li [2], Ruixue Wang [1,*]

[1] School of Science, Jinling Institute of Technology, Nanjing 210093, China;
[2] Guangdong Provincial Key Laboratory of Electronic Functional Materials and Devices, Huizhou University, Huizhou 516001, China
* Correspondence: wrx@jit.edu.cn

Received: December 4, 2025; Accepted: January 16, 2026

Abstract: The upconversion photoluminescence properties of $CaBi_4Ti_4O_{15}$ ceramics co-doped with Yb^{3+}, Ho^{3+} ions were investigated, aiming at their potential application in temperature sensing. X-ray diffraction confirmed the successful synthesis and pronounced textured characteristics of the ceramics. Under 980 nm laser excitation, the $CaBi_{3.96-x}Yb_{0.04}Ho_xTi_4O_{15}$ (x = 0.01, 0.02, 0.03, 0.04) textured ceramics exhibited three distinct emission bands at 549 nm, 660 nm and 759 nm, corresponding to the transitions $^5F_4 \rightarrow {}^5I_8$, $^5F_5 \rightarrow {}^5I_8$ and $^5F_5 \rightarrow {}^5I_6$ of Ho^{3+} ions. Emission intensities increased with Ho^{3+} concentration, suggesting the absence of concentration quenching. Power-dependent studies confirmed two-photon processes as the origin of three emission bands. Temperature-dependent measurements revealed monotonic thermal quenching, with $CaBi_{3.93}Yb_{0.04}Ho_{0.03}Ti_4O_{15}$ showing the strongest decrease in fluorescence intensity. Luminescence analysis showed near-infrared emission at 759 nm delivered the highest sensitivity, achieving maximum absolute sensitivity of 0.0072 K^{-1} and relative sensitivity of 1.71% K^{-1}. These results demonstrate that Yb^{3+}, Ho^{3+} co-doped $CaBi_4Ti_4O_{15}$ textured ceramics are promising candidates for luminescence-based temperature sensing applications.

Keywords: upconversion; Ho^{3+}; temperature sensing; $CaBi_4Ti_4O_{15}$; textured ceramics

1. Introduction

Luminescent materials doped with trivalent lanthanide rare-earth ions have attracted significant attention due to their distinctive spectroscopic properties, which include upconversion and downshifting spectral conversion [1–5]. Upconversion is a nonlinear optical process whereby two or more photons are absorbed, leading to the emission of a single photon with higher energy [6]. In this process, the incident long-wavelength radiation is converted to the shorter-wavelength, a feature characteristic of the anti-Stokes process. The downshifting process represents another optical phenomena in which a single high-energy photon is absorbed and subsequently re-emitted as a photon of lower energy [7]. In the downshifting process, the short-wavelength radiation is converted into longer-wavelength emission, a feature of Stokes process. In recent years, driven by the potential applications in bio-imaging, photovoltaics, solid-state lasers, optical anti-counterfeiting, optical information storage, and luminescence-based temperature sensing, the upconversion photoluminescence has emerged as a prominent research focus in the field of photonics [8–13]. Among these applications, temperature sensing based on the upconversion photoluminescence has gained considerable attention as an effective thermometry technique, offering distinct advantages such as non-invasive operation and immunity to electromagnetic interference [8]. The luminescence-based temperature sensing technique exploits temperature-dependent characteristics of emission

spectra, including fluorescence intensity ratios, normalized emission intensities, positions of emission peaks, and lifetimes [8–13].

To explore the mechanism of temperature sensing in the luminescent materials for enhancing the sensitivity, researchers developed various upconversion luminescent materials, including single crystals, polycrystalline ceramics and nanoparticles with different rare-earth ion dopants and host matrix. Liu et al. fabricated the Yb^{3+}, Er^{3+} co-doped $Sr_5(PO_4)_3F$ transparent ceramics and investigated the chromatically adjustable upconversion emission and luminescence thermometry based on the thermal coupled energy levels [14]. Ren et al. developed Yb^{3+}, Er^{3+} co-doped $Gd_3Sc_2Al_3O_{12}$ single crystal and achieve dual-mode luminescence thermometry [15]. Wei et al. reported the multiple luminescence intensity ratio thermometers based on both thermal coupled and non-thermal coupled energy levels of Ho^{3+}, Tm^{3+} co-activated $Na_3Y_9F_{32}$ single crystal [16]. Stamenković et al. optimized the quantum yield for upconversion photoluminescence and explored the luminescence intenisty ratio based thermometry of Tm^{3+} activated $SrGd_2O_4$ nanoparticles via the emissions resulting from thermal coupled Stark sub-levels [17]. Among various trivalent lanthanide activators, Ho^{3+} ions are particularly appealing for upconversion applications due to the uique energy level structure, enabling strong green, red and infrared emissions in a wide wavelength range [18]. When co-doped with sensitizers such as Yb^{3+} ions, Ho^{3+} ions exhibit enhanced fluorescence intensity resulting from efficient energy transfer, making them highly suitable for luminescence thermometry [19].

The choice of host matrix significantly influences both sensitivity and operational range of luminescence thermometry [9,20]. Compared with the common fluoride matrices, oxide matrices have the advantages of non-toxicity and high thermal and chemical stability. $CaBi_4Ti_4O_{15}$, a representative Aurivillius-type ferroelectric oxide, has unique layered crystal structure, composed of alternately stacked $[Bi_2O_2]^{2+}$ layers and perovskite blocks, produces a structurally anisotropic lattice with large A-site cations and octahedrally coordinated B-site cations, thereby providing a versatile crystal field environment for accommodating rare-earth dopants. This architecture facilitates the incorporation of sensitizer and activator ions, enabling efficient energy transfer and stable upconversion luminescence. Few studies have reported on its ferroelectric and piezoelectric properties achieved through doping, composite construction, and texture control [21,22]. However, little attention has been paid to its luminescent performance and luminescence-based temperature sensing when doped with rare-earth ions. This research gap provides an opportunity to explore the optical functionalities of $CaBi_4Ti_4O_{15}$ while fully leveraging the inherent advantages of oxide matrices in luminescence thermometry. Compared with conventional oxide hosts such as vanadates and molybdates, $CaBi_4Ti_4O_{15}$ offers several distinctive advantages, including a flexible layered framework that ensures structural stability even at relatively high doping concentrations. Additionally, the intrinsic anisotropy allows for controllable orientation (texturing), which is not feasible in most vanadates and molybdates hosts.

In this work, textured $CaBi_4Ti_4O_{15}$ ceramics with varying Ho^{3+} concentrations were fabricated through a combination of molten salt synthesis and solid-state sintering. Analysis of structural characteristics verified that Yb^{3+} and Ho^{3+} ions are readily incorporated into lattice, attributed to their ionic size and valence similarity to Bi^{3+} ions. The effects of Ho^{3+} content, excitation power and temperature on photoluminescence properties were systematically assessed. Furthermore, the temperature sensing properties of three characteristic upconversion emission bands under 980 nm laser excitation were evaluated using a thermal quenching model.

2. Materials and Methods

2.1. Materials Synthesis

Yb^{3+}, Ho^{3+} co-doped $CaBi_4Ti_4O_{15}$ powders with nominal composition of $CaBi_{3.96-x}Yb_{0.04}Ho_xTi_4O_{15}$ ($x = 0.01, 0.02, 0.03, 0.04$) were synthesized via the molten salt method. Stoichiometric amounts of raw materials, including $CaCO_3$, Bi_2O_3, TiO_2, Yb_2O_3 and Ho_2O_3 were weighted according to the target compositions. NaCl and KCl were weighed in a 1:1 mass ratio and thoroughly mixed with the

reactants and an appropriate amount of anhydrous ethanol. The mixtures were ball milled at 300 r /min for 10 h in a nylon jar. The resulting slurry was dried at 120 ℃ in an oven. The dried mixtures were placed in a corundum crucible, and calcined at 850 ℃ for 5 h in a muffle furnace to achieve the molten salt reaction. The heating rate is 5 ℃ /min in the process of powder calcination. After calcination, the NaCl and KCl salts were removed by washing the resulting powders with deionized water preheated to 60 ℃, followed by vacuum filtration. Filtration was performed using slow-flow quantitative filter paper with a pore size of 1–3 μm and the powders were thoroughly washed multiple times, gently resuspending between filtrations. After multiple rounds of washing and filtration, the insoluble products were collected and dried for the ceramics fabrication. The dried powders were mixed with a few drops of polyvinyl alcohol (PVA) binder and uniaxially pressed into disc-shaped pellets with diameter of 13 mm. For removing the binder, the green compacts were heated at 550 ℃ and held for 1 h in muffle furnace. The pellets were then sintered at 1200 ℃ for 2 h and cooled naturally to obtain the dense ceramics. The heating rate for sintering process is 5 ℃ /min.

2.2. Characterization

The phase structure and crystal orientation of the synthesized ceramic samples were examined by X-Ray diffraction (XRD). Upconversion photoluminescence (UCL) spectra of ceramics were excited using a power-adjustable 980 nm semiconductor laser and collected with a fibre-optic spectrometer. The spectral acquisition range was from 400 nm to 800 nm. To examine the excitation power dependence, the UCL spectra were recorded for each sample under a 980 nm laser excitation with different excitation powers. Additionally, the temperature-dependent UCL of ceramic samples with different compositions were investigated under a fixed excitation power of 200 mW. The samples were heated using a programmable heating stage, and UCL spectra were recorded at an interval of 20 K during the heating process, enabling systematic evaluation of optical response to temperature variations.

3. Results and Discussion

To investigate the structural characteristics of the synthesized $CaBi_4Ti_4O_{15}$ ceramics, XRD patterns were recorded. As shown in Figure 1 (a), the diffraction profiles of $CaBi_{3.96-x}Yb_{0.04}Ho_xTi_4O_{15}$ (x = 0.01, 0.02, 0.03, 0.04) ceramics exhibit the similar features, containing a series of sharp diffraction peaks with similar relative intensities and positions. These diffraction peaks can be indexed to (00L) reflections, including (006), (008), (00$\underline{10}$), (00$\underline{12}$), (00$\underline{14}$), (00$\underline{16}$), (00$\underline{18}$) and (00$\underline{20}$), demonstrating that the synthesized ceramics possess pronounced textural characteristics [23]. No additional phases associated with Yb^{3+} and Ho^{3+} doping ions were detected in the diffraction patterns, suggesting that the rare-earth ions were incorporated into host lattice within the experimental doping concentration range. Figure 1 (b) displays the enlarged view of the most intense (00$\underline{10}$) diffraction peaks. As shown, a slight shift in peak position occurs with increasing Ho^{3+} concentration. With Ho^{3+} doping concentration increases, the (00$\underline{10}$) diffraction peak initially shifts slightly toward lower angles, and with further doping, the peak then shifts toward higher angles. The observed subtle peak shift can be attributed to the substitution of the smaller rare earth ions for larger Bi^{3+} ions, which initially leads to a lattice expansion along the c-axis. With further doping, the continuous reduction in the average ionic radius of the perovskite layers results in lattice contraction.

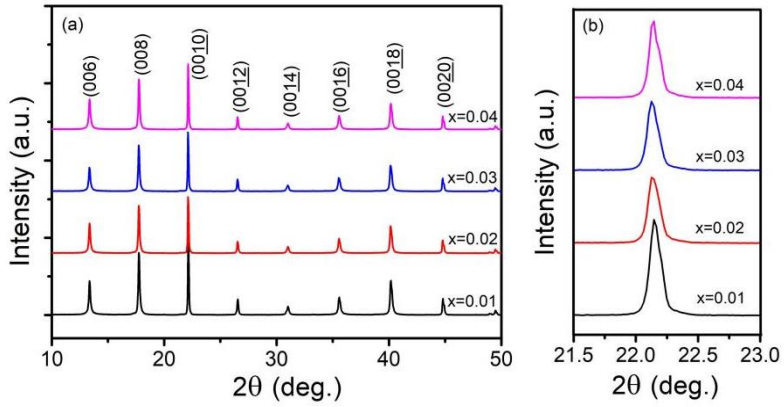

Figure 1. Structural characteristics of Yb^{3+}, Ho^{3+} co-doped $CaBi_4Ti_4O_{15}$ textured ceramics (a) XRD patterns of Yb^{3+}, Ho^{3+} co-doped $CaBi_4Ti_4O_{15}$ textured ceramics with varying Ho^{3+} concentrations; (b) enlarged view of the most intense (0010) diffraction peaks.

The interplanar spacing (d-spacing) of the (0010) plane can be calculated using following Bragg's law,

$$n\lambda = 2d\sin\theta \tag{1}$$

Based on the experimental XRD results of synthesized $CaBi_{3.96-x}Yb_{0.04}Ho_xTi_4O_{15}$ ceramic samples, the calculated d-spacings of the (00$\underline{1}$0) plane are 4.0105, 4.0136, 4.0141 and 4.0111 Å for x = 0.01, 0.02, 0.03 and 0.04, respectively. The evolution in d-spacing confirms the variation in Ho^{3+} ions doping concentration effectively induce a subtle modulation of the lattice structure.

For quantitatively evaluating the degree of preferred orientation in the $CaBi_{3.96-x}Yb_{0.04}Ho_xTi_4O_{15}$ ceramics, Lotgering factors were determined by the following formulas,

$$F = \frac{P - P_0}{1 - P_0} \tag{2}$$

$$P = \frac{\sum I(00L)}{\sum I(HKL)} \tag{3}$$

$$P_0 = \frac{\sum I_0(00L)}{\sum I_0(HKL)} \tag{4}$$

where F is the Lotgering factor, representing the degree of preferred orientation along $(00L)$ direction. P represents the relative intensity ratio calculated from experimental XRD profile. $I(00L)$ and $I(HKL)$ are XRD peak intensities corresponding to the $(00L)$ and (HKL) planes of the measured samples. $I_0(00L)$ and $I_0(HKL)$ are the peak intensities of $(00L)$ and (HKL) planes from the standard PDF card No. 52–1640.

The values of F for synthesized $CaBi_{3.96-x}Yb_{0.04}Ho_xTi_4O_{15}$ ceramics with x = 0.01, 0.02, 0.03 and 0.04 are determined to be 0.918, 0.913, 0.916 and 0.917, respectively.

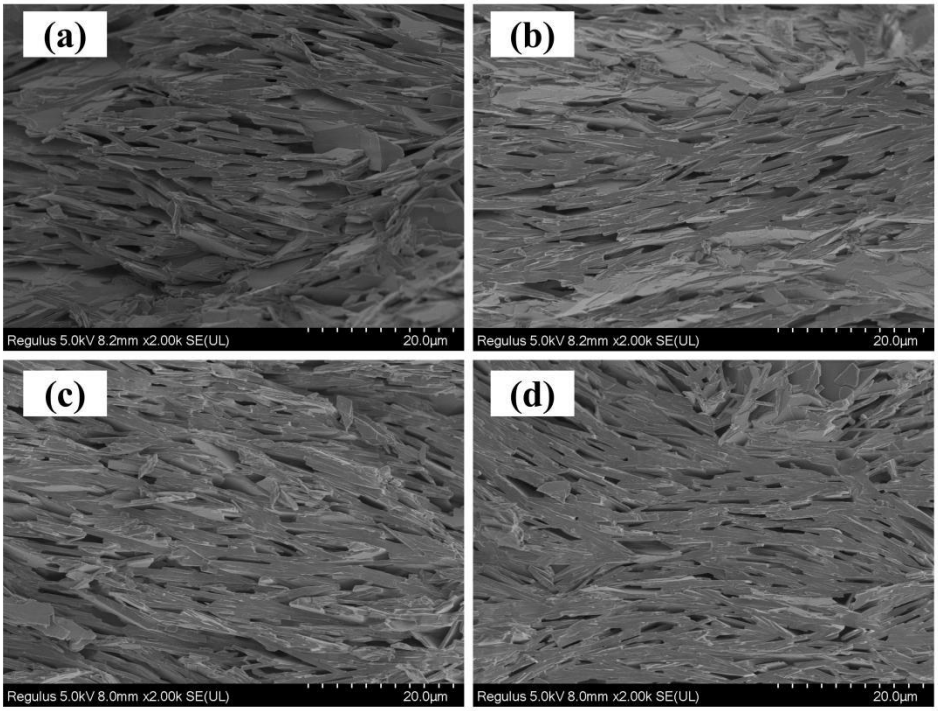

Figure 2. SEM images of the synthesized $CaBi_{3.96-x}Yb_{0.04}Ho_xTi_4O_{15}$ ceramic cross-sections corresponding to x = (a) 0.01; (b) 0.02; (c) 0.03; (d) 0.04 (Scale bar: 20 μm).

The morphology of the Yb^{3+}, Ho^{3+} co-doped $CaBi_4Ti_4O_{15}$ ceramics were investigated using scanning electron microscopy (SEM). Figure 2 (a)–(d) present the SEM images of the $CaBi_{3.96-x}Yb_{0.04}Ho_xTi_4O_{15}$ ceramic cross-sections corresponding to x = 0.01, 0.02, 0.03 and 0.04, respectively. As seen, the cross-sectional SEM images reveal the plate-like grains are aligned along the thickness direction, forming a well-defined lamellar stacking morphology, thereby indirectly confirming the pronounced textural orientation, which is consistent with the preceding XRD analysis.

Yb^{3+} ions were employed as the sensitizers at a fixed concentration, while the concentration of activator Ho^{3+} ions were varied. The upconversion emission spectra of textured ceramics with nominal composition of $CaBi_{3.96-x}Yb_{0.04}Ho_xTi_4O_{15}$ (x = 0.01, 0.02, 0.03, 0.04) were recorded in the wavelength range from 400 nm to 800 nm upon the excitation of continuous-wave 980 nm laser with fixed pump power at 200 mW, as shown in Figure 3 (a). The upconversion emission spectra revealed three distinct emission bands peaked at 549 nm, 660 nm, and 759 nm, corresponding to the transitions of $^5F_4 \rightarrow {}^5I_8$ (Green emission), $^5F_5 \rightarrow {}^5I_8$ (Red emission), and $^5F_5 \rightarrow {}^5I_6$ (Infrared emission) of Ho^{3+} ions, respectively. The red emission band at 660 nm exhibits the highest emission intensity for all the four groups of textured ceramics. Figure 3 (b) shows the variation in the integrated intensities of three emission bands as a function of the concentration of Ho^{3+} ions. Within the investigated doping range, the emission intensity exhibits a monotonic increase with increasing dopant concentration. The result indicates the concentration quenching were not observed within the selected doping range, although this phenomenon may occur at higher doping concentrations [18].

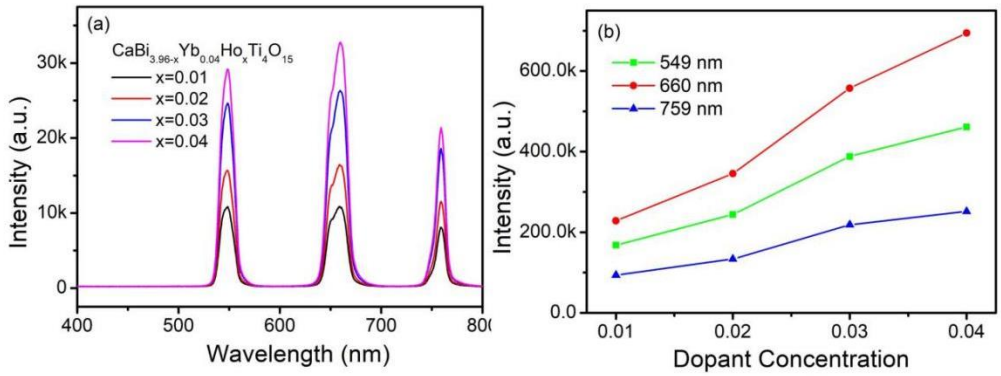

Figure 3. Upconversion emission spectra of Yb^{3+}, Ho^{3+} co-doped $CaBi_4Ti_4O_{15}$ textured ceramics under 980 nm excitation (a) upconversion emission spectra of ceramics with different Ho^{3+} concentrations; (b) dopant concentration-dependent integrated intensities of three emission bands.

To further elucidate the mechanism of upconversion photoluminescence of the textured ceramics, the dependence of emission on excitation power was investigated. Figure 4 (a)–(d) present the upconversion emission spectra of different textured ceramics under identical testing conditions, with excitation power varying from 200 mW to 600 mW. It can be observed that the positions of the emission peaks remain unchanged with excitation power, while the emission intensity increases significantly. The dependence of emission intensity on excitation power can be described by the following relationship [24],

$$I \propto P^n \tag{5}$$

where I represents the emission intensity, P is the excitation power, and n is the number of photons involved in the excitation process [24].

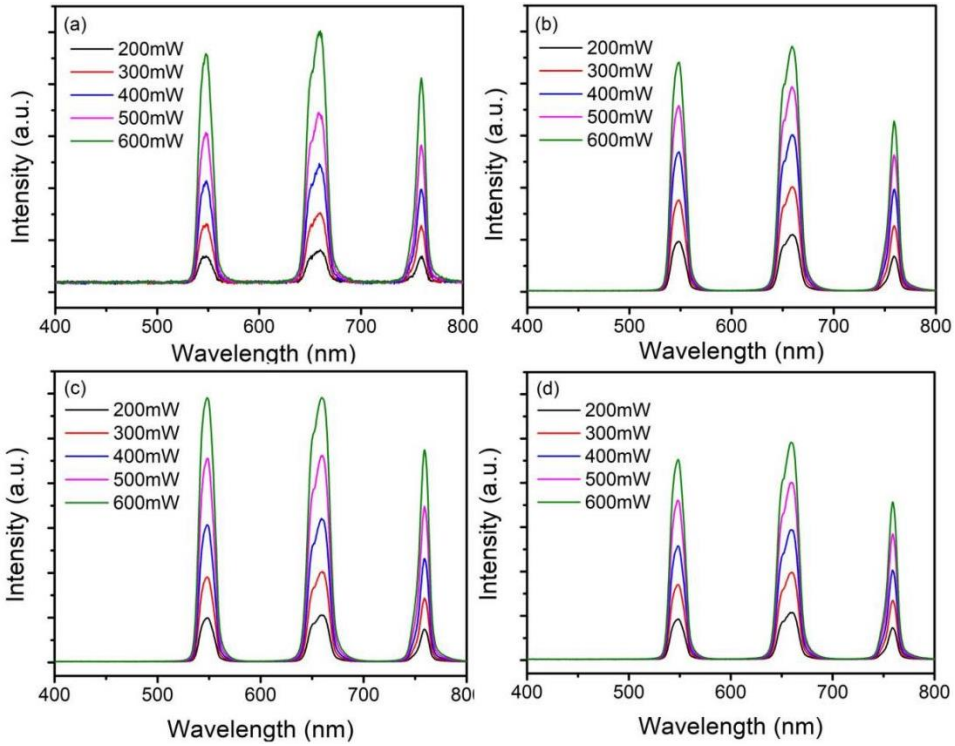

Figure 4. Power-dependent upconversion emission spectra of $CaBi_{3.96-x}Yb_{0.04}Ho_xTi_4O_{15}$ textured ceramics with x = (a) 0.01, (b) 0.02, (c) 0.03, (d) 0.04.

Based on the power-dependent emission spectra, the luminescence mechanism can be analyzed by plotting the dual-logarithmic coordinates of I and P. Figure 5 (a)–(d) present the experimental plots of logI versus logP along with the corresponding linear fitting results for green, red and near-infrared upconversion emissions of different textured ceramics. The slopes obtained from the linear fits represent the numbers of photons participating in the respective upconversion processes. For $CaBi_{3.95}Yb_{0.04}Ho_{0.01}Ti_4O_{15}$, the slopes for green, red, and near-infrared emissions are 2.03, 1.87 and 1.84, respectively. For $CaBi_{3.94}Yb_{0.04}Ho_{0.02}Ti_4O_{15}$, the corresponding slopes are 1.42, 1.37 and 1.48. In the case of $CaBi_{3.93}Yb_{0.04}Ho_{0.03}Ti_4O_{15}$, the corresponding slopes are 1.70, 1.64 and 1.74, whereas for $CaBi_{3.92}Yb_{0.04}Ho_{0.04}Ti_4O_{15}$, the slopes are 1.49, 1.44 and 1.50. The slope values lie between 1 and 2 due to competing linear decay processes occurring during the upconversion process [25]. These results indicate that two-photon processes are responsible for the green, red and near-infrared emissions under 980 nm laser excitation in all investigated Yb^{3+}, Ho^{3+} co-doped $CaBi_4Ti_4O_{15}$ textured ceramics. At specific Ho^{3+} doping concentration, the significant decrease of the slopes can be explained by the in-band $^2F_{5/2}$ of Yb^{3+} becomes more efficiently depleted due to the enhanced $Yb^{3+} \rightarrow Ho^{3+}$ energy transfer. This leads to partial saturation of the first step of the two-step upconversion process under the applied excited power. The population growth rate of intermediate level in these phosphors can be reduced by the saturation.

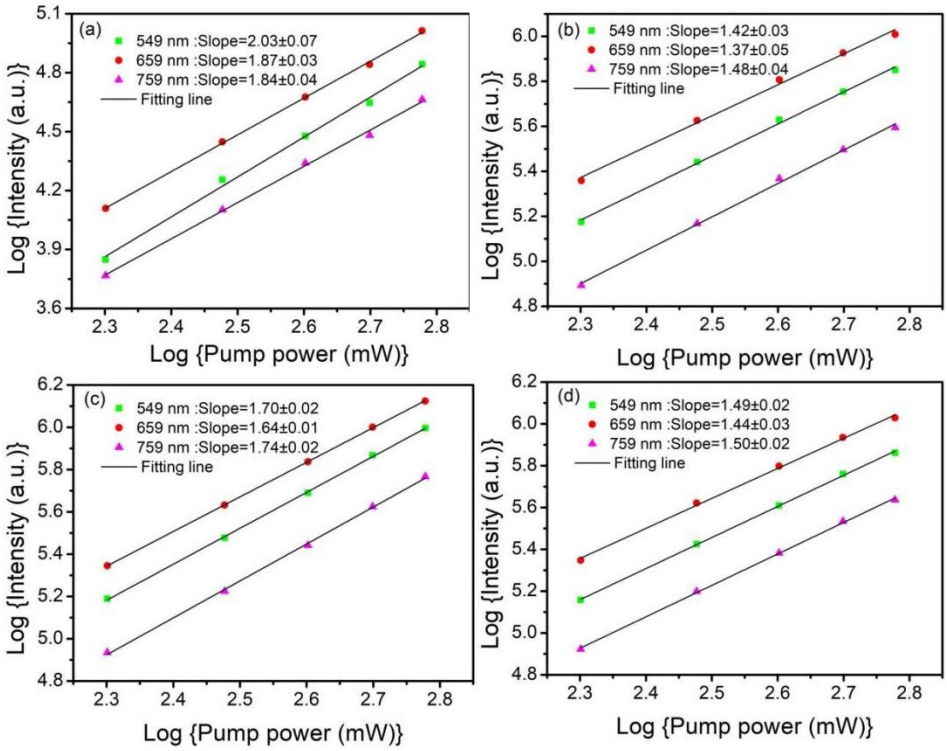

Figure 5. Dual-log plots of upconversion emission intensity versus excitation power at 549 nm, 660 nm and 759 nm for $CaBi_{3.96-x}Yb_{0.04}Ho_xTi_4O_{15}$ textured ceramics with x = (a) 0.01; (b) 0.02; (c) 0.03; (d) 0.04.

To shed light on the effect of temperature on upconversion photoluminescence of the synthesized textured ceramics, the temperature-dependent emission spectra of $CaBi_{3.96-x}Yb_{0.04}Ho_xTi_4O_{15}$ (x = 0.01, 0.02, 0.03, 0.04) were recorded upon excitation of 980 nm laser with a fixed excitation power of 200 mW. Figure 6 (a)–(d) present the emission spectra in range from 400 nm to 800 nm collected over the temperature range of 303 K to 503 K. It can be clearly observed that, for all four investigated compositions, the fluorescence intensities of three characteristic emission bands decrease monotonically with increasing temperature. By comparing the intensities of emission bands, it is evident that the $CaBi_{3.93}Yb_{0.04}Ho_{0.03}Ti_4O_{15}$ ceramic exhibits the largest variation in luminescence

intensity within the investigated temperature range, indicating the most significant fluorescence thermal quenching and highlighting its suitability for luminescence-based temperature sensing.

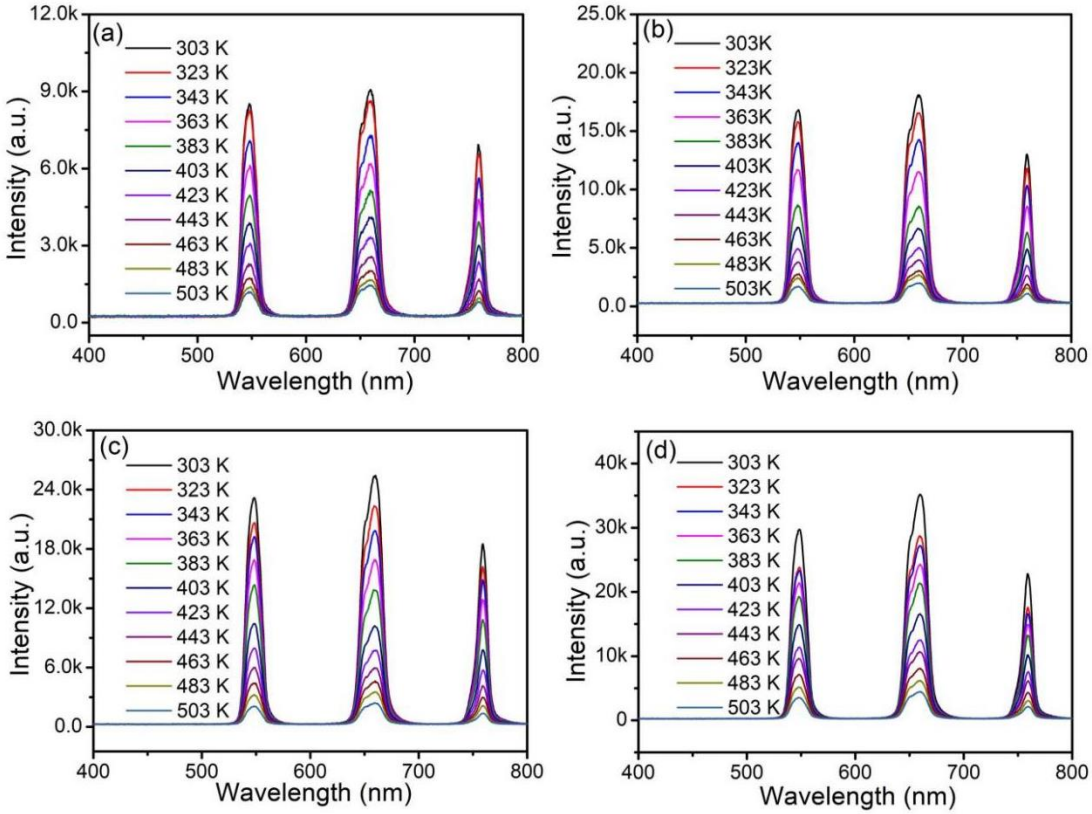

Figure 6. Temperature-dependent emission spectra of $CaBi_{3.96-x}Yb_{0.04}Ho_xTi_4O_{15}$ ceramics under excitation of 980 nm laser for x = (a) 0.01; (b) 0.02; (c) 0.03; (d) 0.04.

To quantitatively investigate the response of fluorescence intensity to temperature variation and gain deeper insight into the thermal quenching behavior of $CaBi_{3.93}Yb_{0.04}Ho_{0.03}Ti_4O_{15}$ textured ceramic, the relationship between temperature and normalized integrated intensities of the three distinct emission bands was analyzed. The basis for analysis of the observed temperature-dependent luminescence characteristics can be described via the following Arrhenius Equation (6) [26],

$$I(T) = \frac{I_0}{1 + Cexp(-\frac{\Delta E}{kT})} \tag{6}$$

where $I(T)$ represents the integrated emission intensity at the T K, I_0 corresponds to the integrated emission intensity at 0 K, C represents the fitting coefficient, k is Boltzmann constant, ΔE denotes the activation energy associated with thermal quenching [26]. Figure 7 (a)–(c) illustrate the temperature-dependent normalized integrated intensities for the emission bands at 549 nm, 650 nm and 759 nm of $CaBi_{3.93}Yb_{0.04}Ho_{0.03}Ti_4O_{15}$ textured ceramic, along with the corresponding fitted curves. For normalization, the emission intensity for each band was divided by the value recorded at 303 K. According to the fitting analysis, the thermal quenching activation energies for 549 nm, 650 nm and 759 nm emission band were determined to be 0.36, 0.31 and 0.37 eV, respectively.

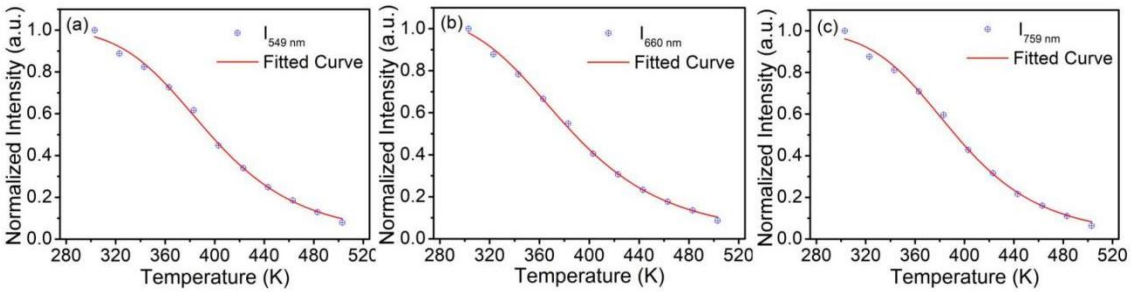

Figure 7. Normalized emission intensity as a function of temperature for $CaBi_{3.93}Yb_{0.04}Ho_{0.03}Ti_4O_{15}$ textured ceramic at (a) 549 nm; (b) 660 nm; (c) 759 nm emission.

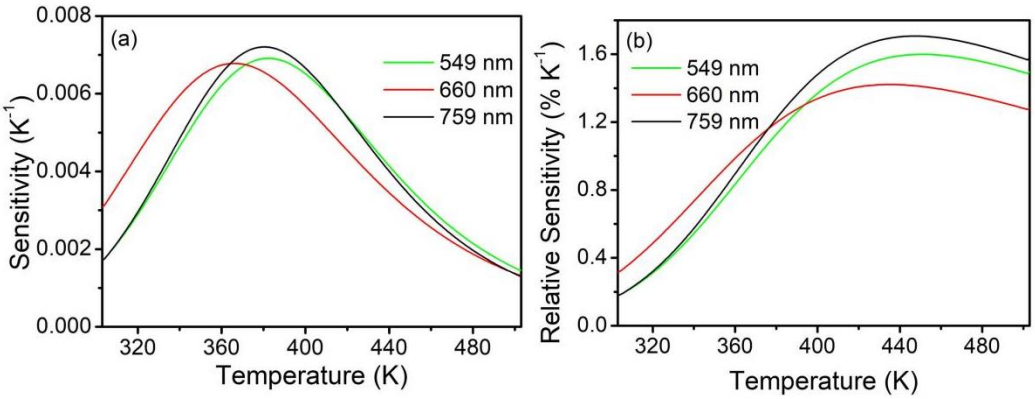

Figure 8. Absolute and relative sensitivity characteristics of $CaBi_{3.93}Yb_{0.04}Ho_{0.03}Ti_4O_{15}$ textured ceramic for optical thermometry based on fluorescence intensity (a) absolute sensitivity; and (b) relative sensitivity.

Sensitivity plays a critical role in evaluating the performance of synthesized luminescent textured ceramics in luminescence-based temperature sensing. Two sensitivity metrics, including absolute sensitivity (S_a) and relative sensitivity (S_r), are commonly employed for such assessments. The values of S_a and S_r can be defined by the following Equations (7) and (8), respectively [11].

$$S_a = \left|\frac{dI(T)}{dT}\right| \tag{7}$$

$$S_r = \frac{1}{I(T)}\left|\frac{dI(T)}{dT}\right| \times 100\% \tag{8}$$

As defined in Equations (3) and (4), S_a quantifies the change in fluorescence intensity per unit temperature variation, while the S_r expresses the change as a percentage of the intensity at the corresponding temperature. Figure 8 (a) presents the temperature-dependent S_a of luminescence thermometry based on three upconversion emission bands of $CaBi_{3.93}Yb_{0.04}Ho_{0.03}Ti_4O_{15}$ textured ceramic under 980 nm excitation. It can be observed that, for each upconversion emission bands, the S_a exhibits an initial ascent with increasing temperature, followed by a descent as the temperature continues to increase. The maximum values of S_a based on the 549 nm, 660 nm and 759 nm emission bands are 0.0069 K^{-1}, 0.0068 K^{-1} and 0.0072 K^{-1}, occurring at 382 K, 366 K and 380 K respectively. The S_r curves exhibit similar trends, increasing first and then declining with temperature, as shown in Figure 8 (b). The S_r for the 549 nm, 660 nm and 759 nm emission bands reach the maximum values of 1.60% K^{-1}, 1.42% K^{-1} and 1.71% K^{-1}, attained at 451 K, 436 K and 447 K, respectively. Among the three emission bands, the near-infrared emission at 759 nm demonstrates the best performance of luminescence thermometry within the investigated temperature range. These results indicate that Yb^{3+}, Ho^{3+} co-doped $CaBi_4Ti_4O_{15}$ textured ceramics hold promising potential for luminescence-based temperature sensing applications.

4. Conclusions

In conclusion, the Yb^{3+}, Ho^{3+} codoped $CaBi_4Ti_4O_{15}$ ceramics were successfully synthesized via a molten salt method followed by solid state sintering. Based on both XRD analysis and microstructural observations, the synthesized ceramics exhibit pronounced textural characteristics. The upconversion luminescence of the synthesized textured ceramics under 980 nm excitation was confirmed to be governed by a two-photon process. Temperature-dependent spectra revealed significant monotonic thermal quenching in all three emission bands with the near-infrared emission at 759 nm demonstrating the optimal S_a of 0.0072 K^{-1} at 380 K and S_r of 1.71% K^{-1} at 447 K. These findings highlight the strong potential of the synthesized Yb^{3+}, Ho^{3+} codoped $CaBi_4Ti_4O_{15}$ textured ceramics for luminescence-based temperature sensing.

Acknowledgments: Not applicable.

Availability of Data and Materials: The datasets generated and analyzed during the current study are available from the corresponding author upon reasonable request.

Funding: This work is funded by Guangdong Provincial Key Laboratory of Electronic Functional Materials and Devices (EFMD2024012M), Research Start-up Program of Jinling Institute of Technology (jit-b-202054) and the Key Discipline Construction Project for Physics at Jinling Institute of Technology.

Author Contributions: Conceived, designed, conducted the experiments, ZL; analyzed the data and wrote the paper, ZL; contributed reagents, ZL; performed data analysis, KL; contributed reagents, KL; conducted the experiments, RXW; analyzed the data, RXW; handled review and editing, RXW; contributed reagents, RXW. All authors contributed to editorial changes in the manuscript. All authors read and approved the final manuscript. All authors have participated sufficiently in the work and agreed to be accountable for all aspects of the work.

Conflicts of Interest: The authors declare no conflict of interest.

References

1. Wei, D.; Fang, L.Z.; Zhou, X.; et al. Enhanced up-conversion luminescence in $Na_5Y_9F_{32}$: Ho^{3+}/Yb^{3+}/Eu^{3+} single crystals by introducing of Gd^{3+} ions for highly sensitive temperature sensing. *Materials Today Chemistry* 2024, 36. https://doi.org/10.1016/j.mtchem.2024.101970
2. Srimathy, B.; Ramesh, B.P.; Rachana, S.; et al. Preparation of Er, Nd Codoped Y_2O_3 Transparent Ceramics and their Upconversion and Downconversion Mechanisms. *Brazilian Journal of Physics* 2025, 55. https://doi.org/10.1007/s13538-025-01694-0
3. Liu, Z.; Chen, D.H. Upconversion photoluminescence and dual-mode temperature sensing properties of PIN-PMN-PT:Er^{3+} ceramic. *Journal of Alloys and Compounds* 2020, 815. https://doi.org/10.1016/j.jallcom.2019.152092
4. Li, Y.H.; Xu, J.H.; Hu, T.B.; et al. Synthesis and Upconversion Luminescence Fine-tuning of Yb^{3+}/Ho^{3+}-Doped Indium and Gallium Oxide Nanoparticles. *Inorganic Chemistry* 2024, 63, 17032–17042. https://doi.org/10.1021/acs.inorgchem.4c02701
5. Liu, Z.; Wang, R.X.; Chen, D.H. Dual-mode optical temperature sensing properties of PIN-PMN-PT:Pr^{3+} ceramic based on fluorescence intensity ratios and lifetimes. *Journal of Materials Science: Materials in Electronics* 2022, 33, 3748–3756. https://doi.org/10.1007/s10854-021-07566-y
6. Cervantes, J.L.; Diaz-Torres, L.A.; Elias, J.; et al. Structural, morphological and photoluminescent study of SiO_2-Y_2O_3 doped with Er^{3+} and Yb^{3+} with enhanced Up-conversion emission. *Applied Physics* 2025, 131. https://doi.org/10.1007/s00339-025-08718-1
7. Hasegawa, T.; Takahashi, Y.; Goto, T., et al. Er^{3+}/Tm^{3+} co-doped $Zr_{0.85}Y_{0.15}O_{1.925}$:$Yb^{3+}$ phosphors: dual-mode ratiometric thermometry based on near infrared up-conversion/down-shifting photoluminescence. *Dalton Transactions* 2024, 53, 13617–13627. https://doi.org/10.1039/D4DT01972E
8. Wang, Y.Q., Dong, X.B., Zhang, H.J., et al. Upconversion Luminescence, Laser Heating Effect and Temperature Sensing Properties of β-$BiNbO_4$:Er^{3+}/Yb^{3+}. *Journal of Electronic Materials* 2021, 50, 201–208. https://doi.org/10.1007/s11664-020-08584-y
9. Chen, W.C.; Gao, H.B.; Molokeev, M.S.; et al. Luminescence enhancement effects of CaxSr2–xNb2O7:Er3+,Tm3+ phosphors for temperature sensing and anti-counterfeiting applications. *Journal of Rare Earths* 2025, 43, 1345–1354. https://doi.org/10.1016/j.jre.2024.06.022

10. Lu, Y.; Wang, J.; Wang, G.; et al. Upconversion luminescence and temperature sensing characteristics of $MgAl_2O_4$ spinel doped with Er^{3+} and Yb^{3+} ions. *Scientific Reports* 2025, 15, 10765. https://doi.org/10.1038/s41598-025-95259-5
11. Feng, M.J.; Guo, J.J.; Chen, J.Y.; et al. Four-mode optical thermometry based on Sm^{3+}-doped Lu_2WO_6 self-activated phosphors. *Journal of Rare Earths* 2025, 43, 1812–1820. https://doi.org/10.1016/j.jre.2024.07.026
12. Jiang, G.C.; Wei, X.T.; Zhou, S.S.; et al. Neodymium doped lanthanum oxysulfide as optical temperature sensors. *Journal of Luminescence* 2014, 152, 156–159. https://doi.org/10.1016/j.jlumin.2013.10.027
13. Raza, S.M.E.; Wang, X.Y.; Jin, Y.X.; et al. Improved thermometry via luminescence lifetime ratio of Er^{3+} and Tm^{3+} operated in the biological window. *Optics Express* 2024, 32, 35822–35831. https://doi.org/10.1364/OE.534968
14. Liu, X.W.; Mei, B.C.; Tan, G.L. Investigation of the sensitization effect of Yb^{3+} in Yb, Er co-doped $Sr_5(PO_4)_3F$ transparent ceramics: From single-band red upconversion to temperature sensing behavior. *Journal of the European Ceramic Society* 2024, 44, 7855–7866. https://doi.org/10.1016/j.jeurceramsoc.2024.05.078
15. Ren, H.; Ding, S.J.; Zheng, Y.H.; et al. Optical temperature sensing of Yb,Er:GSAG single crystal in both upconversion and downconversion dual-mode luminescence. *Materials Today Communications* 2024, 39. https://doi.org/10.1016/j.mtcomm.2024.108806
16. Wei, D.; Fang, L.Z.; Xia, H.P.; et al. $Na_5Y_9F_{32}$:Yb^{3+}/Ho^{3+}/Tm^{3+} up-conversion luminescent single crystals for highly sensitive optical temperature sensor. *Chinese Journal of Physics* 2024, 90, 808–822. https://doi.org/10.1016/j.cjph.2024.06.017
17. Stamenković, T.; Dinić I.; Tomić M.; et al. Quantum yield and thermal sensitivity of $SrGd_2O_4$:Yb, Tm up-conversion nanoparticles. *Ceramics International* 2025, 51, 16878–16886. https://doi.org/10.1016/j.ceramint.2024.10.023
18. Liu, Z.; Chen, D.H. Color tunable upconversion luminescence and optical thermometry properties of mixed Gd_2O_3:Yb^{3+}/Ho^{3+}/Er^{3+} nanoparticles prepared via laser ablation in liquid. *Journal of Materials Science: Materials in Electronics* 2020, 31, 9321–9327. https://doi.org/10.1007/s10854-020-03471-y
19. Mohanty, S.; García-Balduz, J.; Alıcı, A.; et al. Toward Upconversion (Yb–Er) and near-Infrared (Yb–Ho–Er, Nd–Yb) Thermometry with Sea Urchin Type $GdPO_4$ Nanoarchitectures. *ACS Applied Materials & Interfaces* 2024, 16, 57580–57595. https://doi.org/10.1021/acsami.4c14043
20. Zhou, J.; Chen, G.H. Up-conversion optical temperature sensing characteristics of new $KBaGd(MoO_4)_3$:Yb^{3+},Ho^{3+} phosphors. *Journal of Rare Earths* 2025, 43, 2090–2099. https://doi.org/10.1016/j.jre.2024.09.018
21. Shen, Z.Y.; Luo, W.Q.; Tang, Y.X.; et al. Microstructure and electrical properties of Nb and Mn co-doped $CaBi_4Ti_4O_{15}$ high temperature piezoceramics obtained by two-step sintering. *Ceramics International* 2016, 42, 7868–7872. https://doi.org/10.1016/j.ceramint.2016.01.112
22. Yin, Z.M.; Liu, T.; Yang, Y; et al. Multi-modal energy harvesting for efficient piezoelectric photocatalytic pollutant degradation using $CaBi_4Ti_4O_{15}$/BiOI heterojunctions with excellent piezoelectric properties. *Journal of Alloys and Compounds* 2025, 1027. https://doi.org/10.1016/j.jallcom.2025.180566
23. Li, G.H.; Tian, G; Zhai, Y.Z.; et al. Textured $CaBi_4Ti_4O_{15}$ ceramics with large piezoelectricity, excellent thermal stability and high resistivity. *Journal of the European Ceramic Society* 2022, 42, 5584–5590. https://doi.org/10.1016/j.jeurceramsoc.2022.06.049
24. Agarwalla, S.K.; Sridhar, G.; Dikshit, B.; et al. Power dependent variation in relative intensities of blue doublets in Tm doped $NaYF_4$ nanocrystalline system. *Journal of Luminescence* 2025, 281, 121153. https://doi.org/10.1016/j.jlumin.2025.121153
25. Kobwittaya, K.; Oishi, Y.; Torikai, T.; et al. Bright red upconversion luminescence from Er^{3+} and Yb^{3+} co-doped ZnO-TiO_2 composite phosphor powder. *Ceramics International* 2017, 43, 13505–13515. https://doi.org/10.1016/j.ceramint.2017.07.056

26. Maheshwari, K.; Rao, A.S. Photoluminescence downshifting studies of thermally stable Dy^{3+} ions doped phosphate glasses for photonic device applications. *Optical Materials* 2022, 129, 112518. https://doi.org/10.1016/j.optmat.2022.112518

© 2026 by the authors. Submitted for possible open access publication under the terms and conditions of the Creative Commons Attribution (CC BY) license (http://creativecommons.org/licenses/by/4.0/).